Electronic Journal of Structural Engineering

Original Article

Cite this: DOI:10.56748/ejse.26869

Received Date: 21 August 2025
Accepted Date: 07 April 2026

1443-9255
https://ejsei.com/ejse

Mechanical Analysis and Optimization of Mine Roadway Support Structure Empowered by Random Optimization Algorithm

Hongqi Jiang [a*]

[a] School of Mechatronic Engineering, Jiangsu Normal University, Xuzhou 221008, China
*Corresponding author: jianghongqi533@163.com

Abstract

The stability of roadway support structures has a significant impact on the economic benefits and personnel production safety of mines. To analyze the stability state of the mining roadway support structure, this study integrates the support anchor rod and rock structure into a stacked support structure for mechanical characteristic analysis. The optimized Back Propagation (BP) network model in the Stochastic Gradient Descent (SGD) algorithm is introduced to predict the range of loosening circle of mine roadway support structure. The input features of the model include rock rebound value, burial depth, degree of joint development, and tunnel span. In the experiment, the absolute value of the prediction error of the research model is in the range of 1.92 cm to 6.10 cm, with the highest error proportion of 4.9%, and the prediction error is lower than that of other models. Based on the prediction results of the loosening circle range, this study optimizes the parameters of the roadway support structure. Before optimization, the maximum settlement of the top rock layer of the Non-Mining Roadway (NMR) and mining roadway is 43.93 mm and 59.81 mm. After optimization, the settlement and maximum settlement of the top rock layer of the NMR and mining roadway decrease to 32.74 mm and 37.66 mm. The experiment shows that the research method can accurately predict the stability of the mine support structure and has a guiding role in optimizing the mine support structure.

Keywords

Mining, Roadway support, Mechanical analysis, BP neural network, Stochastic gradient descent

1. Introduction

The stability of mine tunnels depends on the design of supporting structures, and the instability of tunnel rock layers may lead to the forced interruption of mining production activities, affecting production efficiency and economic benefits (Liu et al., 2022). In predicting the stability of support structures, traditional monitoring equipment is often expensive, which increases the operating costs of mines. Especially in harsh mining environments, data collection equipment is prone to damage, leading to difficulties in data collection (Yao et al., 2023). Meanwhile, traditional monitoring methods may not be able to accurately predict the stability of support structures, resulting in false or missed warning information.

Zhang et al. analyzed the mechanical mechanism of instability after excavation of tunnels in iron ore fault fracture zones and proposed an optimization plan for support. This scheme utilized Fast Lagrangian Analysis of Continua to simulate the stability of surrounding rock under various support methods and conducted on-site tests using a combination of anchor rod support, anchor mesh, and shotcrete. The monitoring results showed that the tunnel deformation has been effectively controlled (Zhang et al., 2023). Yuan et al. analyzed the mechanical mechanism of deformation and instability of coal seam tunnels under strong mining and demonstrated through field investigations and simulation experiments that the deformation of surrounding rock has stage and band-like collapse characteristics. This study suggested that the key to support lies in suppressing initial deformation and therefore proposed a mechanism of thick anchor boundary crossing support, emphasizing the importance of anchor length (Yuan et al., 2022). Dong et al. used software to simulate the fracture and deformation characteristics of surrounding rock in tunnels under different conditions, determined the support form and parameters, and compared the deformation under unsupported and 3 different support conditions. They proposed a combination support method of "anchor rod+anchor cable+metal mesh". Monitoring data showed that this method effectively controlled the large deformation of the roadway, improved the stability of the surrounding rock, and ensured the safety of the roadway (Dong et al., 2022). Ding et al. studied the layout and support design of the bottom coal mining roadway under strong disturbance in Aguo Mine and investigated the reasonable offset and stress distribution of the roadway layout after upper layer mining. They determined a reasonable external offset of 6 meters. The external staggered arrangement and 6-meter arrangement of roadway support methods were reasonable (Ding et al., 2024). Liu et al. proposed a segmented constant resistance anchor rod structure to enhance the dynamic stability of large deformation tunnels under seismic vibration. The preloading segmented setting reduced tension deviation, and its stability has been verified through on-site testing and simulation. In the dynamic deformation test, the anchor rod had a good response to alternating loads, with a maximum tension deviation of less than 8%, demonstrating better stability than traditional anchor rods (Liu & Zhang, 2022). Rabbani et al. optimized the weights and biases of artificial neural networks using grey wolf optimization, enhanced grey wolf optimization, and Harris hawks optimization to form a hybrid model for predicting soil shear strength. The results indicated that the hybrid model had better performance in both prediction training and testing stages, and the total rank value obtained by the model was much higher than that of other developed hybrid models (Rabbani et al., 2024). Meanwhile, Rabbani A et al. also compared the predictive performance of five models, namely extra tree regression, decision tree regression, ridge regression, linear regression, and Bayesian ridge regression, in soil shear strength. The results showed that the additional tree regression model produced good modeling results, outperforming other models (Rabbani et al., 2024). Avci Y et al. studied the influence of the elastic modulus of compacted expanded aggregate pier, raft foundation thickness, and column spacing on settlement. This study optimized and analyzed new goal achievement methods and response surface methods supported by artificial intelligence. The newly developed code, supported by artificial intelligence, automatically selected the most reasonable prediction function and created a prediction function with high a correlation coefficient for optimization analysis (Avci & Ekmen, 2023). Alesmael et al. used a new artificial intelligence-assisted target achievement technique to optimize the process, which generates robust regression functions based on data obtained from 3D finite element analysis of pile raft foundation systems. In multi-objective optimization, a balance was achieved between the parameters of the raft foundation system and reliable settlement to ensure the economic and safe design of the model (Alesmael & Ekmen, 2025).

Han et al. developed an anomaly detection model built on a Genetic Algorithm (GA)-optimized BackPropagation (BP) network that combines Global Navigation Satellite System (GNSS) and accelerometer data. This network cross-verified predicted displacements in a neural network by integrating acceleration in the frequency domain and GNSS displacement trends, for anomaly detection and repair. This method had better anomaly detection performance than other methods, with a single anomaly detection rate of 84.25% and a mixed anomaly detection rate of 73.53% (Han et al., 2025). Xu et al. proposed using an improved BP network to predict the forming quality of alloys during cold radial forging, evaluating parameters based on damage, residual stress, and equivalent strain. Research has shown that the improved BP model outperformed traditional BP and other machine learning techniques in terms of predictive performance, and the optimized process parameters

significantly reduced residual stress, equivalent strain, and component damage (Xu et al., 2024). Wang et al. proposed an improved BP model for residual strength assessment of oil and gas pipelines and introduced relative errors in parameters and pressure ratios to comprehensively analyze its accuracy and applicability. The optimized BP network significantly outperformed traditional BP in convergence speed and system performance (Wang et al., 2024). Li et al. established a 3D transient calculation model for particle oxidation in high-speed oxygen fuel spraying and used an improved BP model to analyze and determine the optimal process parameters. The experiment verified that the optimized coating had fewer defects, lower oxide content, and higher hardness and wear resistance (Li et al., 2025). Li et al. established an improved BP model to determine the optimal parameters for laser cladding technology by changing process parameters, conducting numerical calculations, and obtaining sample data. The optimized process parameters of the improved BP model were laser power of 1076.41 W, spot radius of 2.61 mm, and scanning velocity of 6.05 mm/s. This study provided a theoretical basis for enhancing the quality of the cladding layer (Li et al., 2023).

In summary, there are relatively abundant research results on the stability of mining tunnels, but obtaining stability impact indicators in current research methods often faces practical difficulties. For example, the measurement cost of rock strength indicators and geostress indicators in actual mining conditions is relatively high. Therefore, this study uses the Random Optimization Algorithm (ROA) to empower the BP model and predict the relationship between the influencing indicators and the range of the loosening circle. Given the above issues, the paper proposes a joint approach of Stochastic Gradient Descent (SGD) and BP network (SGD-BP) in ROA for predicting the loosening range of Mine Roadway Support Structures (MRSS). The innovation lies in the combination of the mechanical analysis of MRSS and the deformation of the loose circle of the roadway rock layer, which guides the parameter optimization of the support structure. This study uses the mechanical analysis results of the stacking support structure as the boundary conditions for model prediction and feeds the prediction results back to support parameter optimization, forming a complete technical path for mechanical analysis loosening range prediction and support parameter optimization. This study aims to provide scientific methods for preventing settlement deformation in mining tunnels, thereby promoting safe production in mines.

2. Methods and Materials

To improve the prediction accuracy of MRSS stability, this study constructs an SGD-BP model, which provides boundary conditions for the stability design of support structures through MRSS and mechanical analysis. SDG and BP models are introduced for predicting the range of loose zones in mining tunnels.

2.1 MRSS and mechanical analysis

In mining tunnels, to prevent roof collapse, support structures are often designed to support the rock layers at the top of the tunnel. To address the design of MRSS, this study first analyzes the model and mechanical characteristics of the support structure. In the mining tunnel structure, the length of anchor rods usually exceeds the thickness of the top mining layer. Therefore, anchor rods can penetrate the mining layer and extend into deeper rock layers (Jha, 2025). Through the reinforcement of anchor rods, the support structure can connect and fix the mining layer and deeper rock layers, forming a cohesive support structure. When conducting mechanical analysis, this study considers the top mining layer and rock strata within the range controlled by the anchor rod as a single entity and simplifies it as an anchoring structure with superimposed support. By simplifying the anchoring structure, the working principle and stress characteristics of the support structure can be more clearly understood. The simplified model of the stacked support anchorage structure is shown in Fig.1.

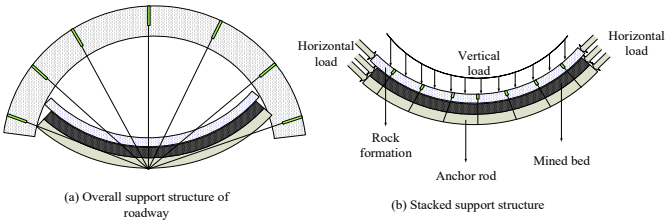

Fig.1 Simplified model of stacked support anchorage structure

Fig.1 (a) shows a simplified anchoring structure where support anchor rods are stacked with rock layers. In Fig.1 (b), the stacked support anchoring structure is divided into three parts: anchor rods, mining layers, and rock layers. When the roadway is subjected to impact, to fix the mining layer below the rock layer, the role of anchor rods is to prevent deformation of the mining layer under various stresses. Therefore, the constraint condition needs to be set to zero bending deflection of the mining layer. Under the above assumptions, the calculation method for the bending moment of the mining layer is given by equation (1).

$$M(x)=\frac{s_1 x}{2}(l-x)+\gamma L_v whw \tag{1}$$

In equation (1), $M(x)$ is the bending moment of the mining layer, x is the position point, l, w, and h are the length, width, and thickness of the mining layer. s_1 is the equivalent uniformly distributed load formed by the vertical load and self-weight of the mining layer. γ is the rock pressure coefficient. L_v and ω are the vertical load and bending deflection of the mining layer. The formula for equivalent uniformly distributed load is shown in equation (2).

$$s_1 = L_v + W_h \cdot h \tag{2}$$

In equation (2), W_h is the unit weight of the mining layer To obtain the deflection distribution of the mining layer under different loads, this study will describe the relationship between bending deflection and bending moment, as shown in equation (3).

$$\frac{d^2\omega(x)}{d^2x}=\frac{M(x)}{EI} \tag{3}$$

In equation (3), d is the differential calculation, E is the elastic modulus, and I is the inertia moment of the cross-section of the mining layer. Afterwards, the differential expression and bending moment calculation formula are combined to obtain the calculation method for the bending deflection of the mining layer, as shown in equation (4).

$$\omega(x)=\alpha\sin\left(\sqrt{\frac{\lambda L_v wh}{EI}}x\right)+\beta\cos\left(\sqrt{\frac{\lambda L_v wh}{E\ I}}x\right)+\frac{s_1 x(x-l)}{2\gamma L_v wh}-\frac{s_1 E\ I}{\lambda^2 L_v{}^2 w^2 h^2} \tag{4}$$

In equation (4), α and β are parameters related to the physical scale of the load and the physical scale of the material. The calculations for both are shown in equation (5).

$$\begin{cases}\alpha=\dfrac{s_1 EI}{\gamma^2 L_v{}^2 w^2 h^2}\left[1/\sin\left(\sqrt{\dfrac{\gamma L_v wh}{EI}}l\right)-\cot\left(\sqrt{\dfrac{\gamma L_v wh}{EI}}l\right)\right]\\ \beta=\dfrac{s_1 EI}{\gamma^2 L_v{}^2 w^2 h^2}\end{cases} \tag{5}$$

By substituting the parameters in equation (5) and the deflection in equation (4) into the bending moment calculation equation, the following equation (6) can be obtained.

$$M(x)=\frac{s_1 EI}{\gamma L_v wh}\tan\left(\sqrt{\frac{\gamma s_1 wh}{4EI}}\right)l*\sin\left(\sqrt{\frac{\gamma s_1 wh}{EI}}x\right)+\frac{s_1 EI}{\gamma L_v wh}*\cos\left(\sqrt{\frac{\gamma s_1 wh}{EI}}x\right)-\frac{s_1 EI}{\gamma L_v wh} \tag{6}$$

After obtaining the bending moment calculation formula, the normal stress calculation of the mining layer can be obtained based on the normal stress formula, as shown in equation (7).

$$s_n(x,y)=\frac{s_1 Ey}{\xi^2}\left[\tan\left(\frac{\xi l}{2\psi}\right)*\sin\left(\frac{\xi}{\psi}x\right)+\cos\left(\frac{\xi}{\psi}x\right)-1\right] \tag{7}$$

In equation (7), $s_n(x,y)$ is the normal stress of the mining layer at position (x,y). ξ is a parameter related to the load and physical dimensions of the mining layer, defined as $\xi=\sqrt{\gamma L_v wh}$. ψ is a parameter related to the material properties and physical dimensions of the beam, defined as $\psi=\sqrt{EI}$. After obtaining the normal stress, the function of the superimposed support structure is to control the deformation of the mining layer and rock layer under various forces through anchor support, so as to satisfy the coordination relationship between bending moment and deformation under different forces, thereby maintaining structural stability (Islavath & Deb, 2022). Therefore, the constraint condition can be defined as the following equation (8).

$$\begin{cases}M(x)=\sum_{i=1}^{n}M_i(x)\\ \sum_{i=1}^{n}L_i=L_v+\sum_{i=1}^{n}W_i h_i-R_s\end{cases} \tag{8}$$

In equation (8), L_i is the equivalent load of the mining layer or rock layer, and R_s is the support resistance. The stacked support structure consists of two layers of rock layers and one mining layer, and the equivalent load calculation of each layer is shown in equation (9).

$$\begin{cases}L_3 &= L_v+W_3h_3-L_{23}\\ L_2 &= L_{23}+W_2h_2-L_{12}\\ L_1 &= L_{12}+W_1h_1-L_O\end{cases} \tag{9}$$

In equation (9), L_1 is the equivalent load of the mining layer. L_{12} is the load transfer between the mining layer and the rock layer. W_1 and h_1 are the weight and thickness of the mining layer. L_O is the force in other vertical directions. L_2 is the equivalent load of the first layer of rock strata. L_{23} is the load transfer between the first and second rock layers. W_2 and h_2 are the weight and thickness of the first layer of rock. L_3 is the equivalent load of the second rock layer. W_3 and h_3 are the weight and

thickness of the second layer of rock. After obtaining the equivalent loads of each layer of the stacked support structure through equation (9), the structural parameters that enable the support structure to achieve deformation coordination can be obtained by combining equation (8).

2.2 Prediction of LZR in roadways by integrating ROA and BP networks

Loose Zone Range (LZR) refers to a circular area where the stress redistribution of the surrounding rock exceeds the strength of the rock mass after excavation, resulting in rock fracture, loosening, and deformation. This area is the main target of the roadway support structure, and its size directly affects the selection of support parameters and the stability of the roadway. After obtaining the optimized boundary conditions of the support structure through mechanical analysis, this study will use the SGD-BP model to further predict the LZR of the roadway. Due to mining activities causing a larger range of rock loosening and deformation, it is necessary to accurately predict the extent of the loosening zone to guide the optimization of the stacked support structure.

Before predicting the range of rock loosening zones in mine tunnels, this study first selects the influencing factor indicators of the range of rock loosening zones in mines. The strength of surrounding rock is one of the main factors affecting the range of loose zones in tunnels, and the strength of surrounding rock is generally measured by uniaxial compressive strength (Zhou et al., 2024). However, in the interior of mining tunnels, the cost of measuring uniaxial compressive strength is high, and the work is complex. Therefore, this study chooses the rock rebound value instead of uniaxial compressive strength to measure the strength of the surrounding rock (Wu et al., 2025). The rebound value of rock mass is an indirect indicator of the strength of the surrounding rock. The higher the rebound value, the greater the strength of the surrounding rock, and the stronger its ability to resist deformation and failure. Therefore, the range of the loosening zone is smaller. Secondly, geostress is also one of the main factors affecting the LZR in tunnels. The greater the geostress, the more likely the surrounding rock is to fracture and deform, leading to an increase in the range of the loosening zone. Similarly, the measurement and acquisition process of geostress is complex, so the study selects burial depths that have a functional relationship with geostress. Specifically, the deeper the burial depth, the higher the level of geostress, and the greater the load borne by the surrounding rock, making it more prone to rupture and deformation, resulting in an increase in the range of the loosening zone. Afterwards, the higher the degree of joint development in the surrounding rock, the more cracks there will be, the lower the strength of the surrounding rock, and the easier it will be to increase the scope of the loose zone (Rabbani et al., 2023). The larger the span, the larger the exposed area of the tunnel roof and both sides, and the self-stabilizing ability of the surrounding rock decreases. Under the same geostress conditions, deformation and failure are more likely to occur, and the range of the loosening zone increases accordingly.

After measuring the above influencing factors, this study integrates ROA and BP networks to evaluate the stability of tunnels during mining processes. To more conveniently obtain the range of loose zones in tunnels and reduce workload, this study uses SGD-BP to construct a prediction model for the LZR. The specific model structure is shown in Fig.2.

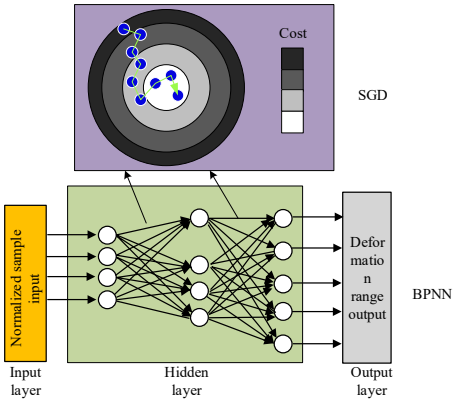

Fig.2 SGD-BP prediction model for LZR of rock strata in mine roadways

In Fig.2, the BP network is a multi-layer feed-forward neural network that performs pattern recognition or prediction by learning the relationship between input data and output data. After receiving input information, the input layer of the network connects the input vector with the hidden layer units through weight parameters. The hidden layer unit also receives an additional input signal threshold to determine whether the neuron should be activated. After the activation function is processed, the output of the hidden layer is calculated and passed to the next layer of the network until the final output layer. Equation (10) shows the output of the hidden layer.

$$X_b = F(\sum_{a=1}^{n} W_{ab} X_a + Q_b) \tag{10}$$

In equation (10), X_a is the input vector. X_b is the output. W_{ab} is the weight. Q_b is the threshold. F is the activation function. a and b are input vector numbers and hidden layer unit numbers. n is the number of input vectors. The output data from the hidden layer enters the output layer for processing. The output method of the output layer is shown in equation (11).

$$Y_c = F(\sum_{b=1}^{q} W_{bc} X_b + Q_c) \tag{11}$$

In equation (11), Y_c is the output value of the c -th unit of the output layer. W_{bc} is the weight between the hidden layer and the output layer. Q_c is the output layer threshold. q is the number of hidden layer units. After obtaining the output value of the loose circle range, the output value can be compared with the expected value to obtain the model error. After obtaining the error, the BP adjusts the model's weights and thresholds through a reverse feedback learning mechanism, and the weight adjustment method is shown in equation (12).

$$\begin{cases} W'_{ab} = W_{ab} + \varphi_i X_b (1 - X_b) X_a \sum_{c=1}^{m} W_{bc} e_c \\ W'_{bc} = \left| W_{bc} + \varphi_i X_b e_c \right| \end{cases} \tag{12}$$

In equation (12), W'_{ab} and W'_{bc} are the adjusted model weights. e is the error, and φ is the network learning rate. The method for adjusting the threshold is shown in equation (13).

$$\begin{cases} Q'_b = Q_b + \varphi_i X_b (1 - X_b) X_a \sum_{c=1}^{m} W_{bc} e_c \\ Q'_c = Q_c + e_c \end{cases} \tag{13}$$

In equation (13), Q'_b and Q'_c are the adjusted model thresholds. The BP algorithm typically uses SGD to adjust weights in neural networks; however, gradient descent algorithms may cause local minimum problems in the model (Li et al., 2024). Therefore, this study introduces the SGD from ROA to optimize the BP network. The weight update of the BP model under SGD is shown in equation (14).

$$W' = W - \varphi \cdot \nabla f(w) \tag{14}$$

In equation (14), W' is the optimized weight of SGD algorithm, W is the weight before optimization, and $\nabla f(w)$ is the weight gradient function. After obtaining the range of rock loosening zones in mine tunnels through the SGD-BP model, this study uses the constraint conditions in equation (8) as the boundary conditions for the optimization model of the support structure. The application process of the optimization model for mine support structure combining ROA and BP network is shown in Fig.3.

In Fig.3, after overlaying the anchoring support structure with the rock layer for mechanical analysis, the deformation coordination relationship between the mining layer and the rock layer is obtained to monitor whether the anchoring structure can play a role (Zhou et al., 2021). To determine whether the anchoring support structure can ensure the roadway's stability during the mining process, this study optimizes the BP model using the SGD algorithm in ROA and constructs a prediction model for the range of the roadway loosening zone. After outputting the loosening range of the roadway, the parameter optimization of the support structure can be guided by constraint conditions to achieve stable mining in the roadway.

Finally, the predictive performance of BP neural networks is highly dependent on the initial weights and threshold settings, and the selection of network structure often relies on experience, which can easily lead to local minima. Therefore, the study introduces GA to optimize BP neural network. The basic idea of GA is to encode the weights and thresholds of BP neural networks into chromosomes, and iteratively evolve them through genetic operations such as selection, crossover, and mutation to find the optimal parameter combination that minimizes network error. When optimizing, it is necessary to encode the weights and thresholds between each connecting unit into chromosomes using real numbers, generate the first-generation population, and then use the roulette wheel method to select individuals. The crossover method is two-point crossover, with a crossover probability of 0.8. Iterative evolution is performed using Gaussian mutation with a probability of 0.2 to obtain the optimal chromosome, and the chromosome is decoded to obtain the optimized weights and thresholds. The weights and thresholds obtained by GA optimization are assigned to each layer unit of the BP neural network as initial values. Then, local optimization of the BP algorithm is achieved by training the model. When training the model with input sample data, the weights and thresholds between each connected unit will be continuously adjusted and corrected based on forward and backward feedback information until the output results meet the error requirements, which is the optimal weight and threshold.

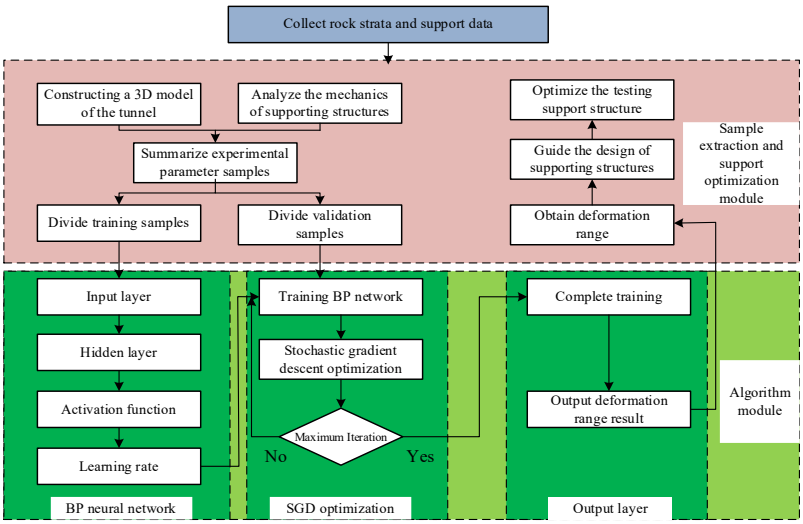

Fig. 3 Application process of SGD-BP mining support structure optimization model

3. Results

To verify the application of the SGD-BP model, this study compared the prediction errors of different models through model parameters and validated its performance in predicting the LZR of mine tunnels.

3.1 LZR prediction performance of the SGD-BP model

This study conducted experiments using an iron mine in Anhui Province, China as a case study. The mine was located in Zhong Guao on the southern edge of Ningwu Diwa in the central China Diwa area, Suzhou-Hubei Diwa system or Qinhuai arc tectonic system. It was in the intense period of the Late Jurassic to Cretaceous Diwa, in the southern section of the Ningwu fault basin, on the east bank of the Yangtze River. The main ore body of iron ore was mainly located in the inner zone of the contact between diorite and sandstone shale, with a dip angle of 5° to 35° on both wings, generally 10° to 30°, and a wavy northward dip angle of about 13°, roughly the same as the dip angle of the anticline. The burial depth of the ore body was below 206 meters, with an occurrence elevation of -200 to -400 meters. Firstly, the impact indicators of LZR were collected. Table 1 shows the specific data.

In Table 1, this study collected data on 26 indicators in different tunnels and collected support structure parameters in mining tunnels. The SGD-BP model was used to predict LZR in tunnels. Table 2 shows the specific support and model parameters.

Table 1. Impact index data of LZR in mining tunnels

Number	Buried depth (m)	Rebound value	Span (m)	Degree of joint development	Number	Buried depth (m)	Rebound value	Span (m)	Degree of joint development
1	320	51.55	6	4	14	365	42.98	6	2
2	320	32.56	6	4	15	390	34.42	6	4
3	320	36.47	4.5	3	16	390	24.28	6	4
4	330	38.07	6	4	17	390	38.46	4.5	3
5	330	46.21	6	2	18	411	31.1	6	3
6	330	40.75	3.6	3	19	411	29.71	6	3
7	330	28.44	4.5	4	20	424	36.73	4.5	3
8	370.5	56.78	4.5	3	21	424	41.61	6	2
9	370.5	38.22	6	4	22	424	34.35	6	3
10	370.5	28.03	6	4	23	432.5	53.59	4.5	2
11	370.5	34.75	6	3	24	432.5	33.41	6	4
12	370.5	47.64	4.5	4	25	432.5	27.89	6	5
13	365	33.55	6	2	26	452.5	43.91	4.5	4

Table 2. Mechanical parameters and model parameters of supporting structures

Mechanical parameters		SGD-BP model's parameter	
Lateral pressure coefficient of surrounding rock	1.5	Number of input layers	4
Vertical load of mining layer	0.8MPa	Hidden layer neuron	5-25
Length of mining layer	5m	Number of output layers	1
Elastic modulus of mining layer	2.33GPa	Learning rate	0.01, 0.005, 0.001
Mining layer width	1m	Activation function	Sigmoid
/	/	Loss function	Euclidean distance

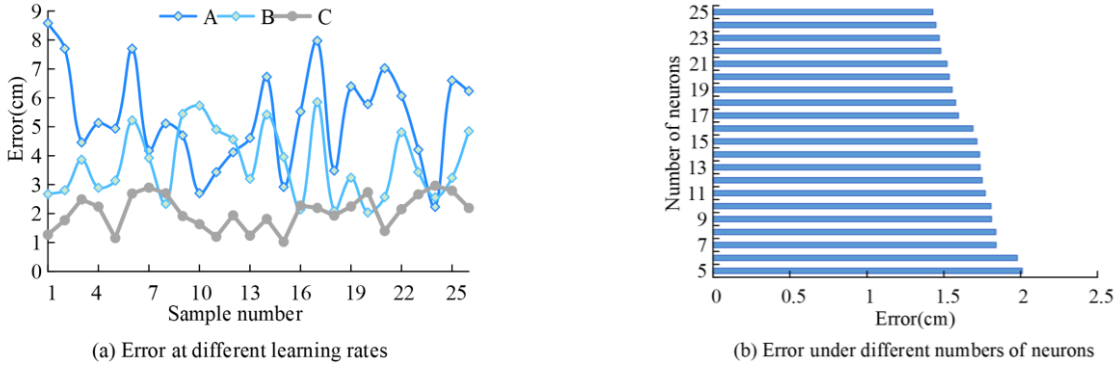

(a) Error at different learning rates

(b) Error under different numbers of neurons

Fig. 4 Experimental error results under different model parameters

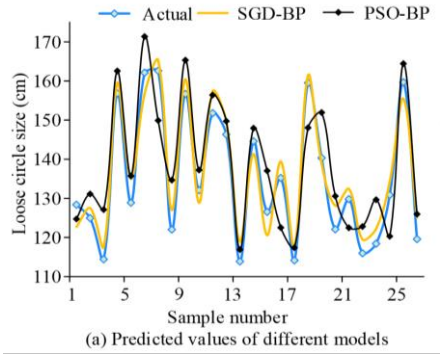

Fig. 5 Prediction error results of different models

In addition to the mining layer parameters in Table 2, the specification of the support anchor rod was 20mm * 1800mm, the diameter was 30 mm, and the spacing between anchor rods was 900mm * 1000mm. To comprehensively evaluate the predictive performance of the SGD-BP model, multiple statistical indicators were used to quantitatively evaluate the model, including Absolute Error (AE) and Mean Absolute Error (MAE). AE refers to the absolute difference between the predicted value of the model and the measured value on site, reflecting the prediction bias of a single sample. The MAE represents the MAE of all samples, reflecting the overall prediction bias level of the model. Based on the above parameters, this study first analyzed experimental errors under various model parameters, as exhibited in Fig.4.

In Fig.4, A, B, and C represent the error situations with learning rates of 0.01, 0.005, and 0.001. When testing the impact of learning rate on error, the number of neurons was 5. When testing the impact of the number of neurons on errors, the learning rate was 0.001. In Fig.4 (a), when the learning rate was 0.01, the model produced a large error result, with an error between 8.5 cm and 2.2 cm and an average error of 5.33 cm. When the learning rate was 0.005, the error was between 5.8 m and 2.0 cm, with an average error of 3.73 cm. When the learning rate was 0.001, the error was between 2.9 m and 1.0 cm, with an average error of 2.06 cm. In Fig.4 (b), as the number of neurons increased from 5 to 25, the average error gradually decreased. When the number of neurons was 25, the model error was the lowest, at 1.43 cm. Therefore, the learning rate of the SGD-BP model was 0.001, and the number of neurons was 25. Afterwards, this study compared the prediction errors of SGD-BP and Particle Swarm Optimization-BP (PSO-BP) models, as shown in Fig.5.

In Fig.5 (a), the absolute value of the prediction error of PSO-BP and SGD-BP was in the range of 3.01cm-12.70cm and 1.92cm-6.10cm. The average prediction error of PSO-BP and SGD-BP was 7.22 cm and 3.91 cm. In Fig.5 (b), the error proportion of PSO-BP was the highest at 11.1%, while that of SGD-BP was the highest at 4.9%. SGD-BP had higher accuracy and smaller errors in mining LZR prediction.

3.2 Optimization experiment of MRSS based on SGD-BP model

After verifying the LZR prediction performance of SGD-BP, this study applied SGD-BP to optimize the support structure of mining tunnels. Based on the parameters of the mine roadway in Table 1, Rhino6 software was utilized to build the roadway model, and the roadway model was imported into FLAC3D software. Based on the analysis of the mechanical characteristics of superimposed support through research, equation (8) was set as the boundary condition for the model. Firstly, this study simulated and optimized the support structure of Non-Mining Tunnels (NMTs). The LZR of Non-Mining Roadway (NMR) rock layers was 0.4m-1.0m. Table 3 shows the experimental parameters for optimizing the support structure under NMTs.

Table 3. Parameters in the optimization experiment of support structure under NMR

Factors and levels					Optimization plan								
Factor	Code	Level1	Level2	Level3	1	2	3	4	5	6	7	8	9
Length (cm)	A	120	140	160	120	120	120	140	140	140	160	160	160
Diameter (mm)	B	16	18	20	16	18	20	16	18	20	16	18	20
Distance (cm)	C	100	110	120	100	120	110	120	110	100	110	100	120
Row spacing (cm)	D	100	110	120	100	110	120	120	100	110	110	120	100

Table 4. Displacement Range Analysis Table

Level	Factor A (mm)	Factor B (mm)	Factor C (mm)	Factor D (mm)
1	66.61	69.58	57.75	54.88
2	63.34	62.06	61.07	62.63
3	62.35	60.66	73.48	74.79
Average level 1	22.20	23.19	19.25	18.29
Average level 2	21.11	20.69	20.36	20.88
Average level 3	20.78	20.22	24.49	24.93
Average range	1.42	2.97	5.34	6.64
Level priority	1>2>3	1>2>3	3>2>1	3>2>1
Primary and secondary factors	D>C>B>A			

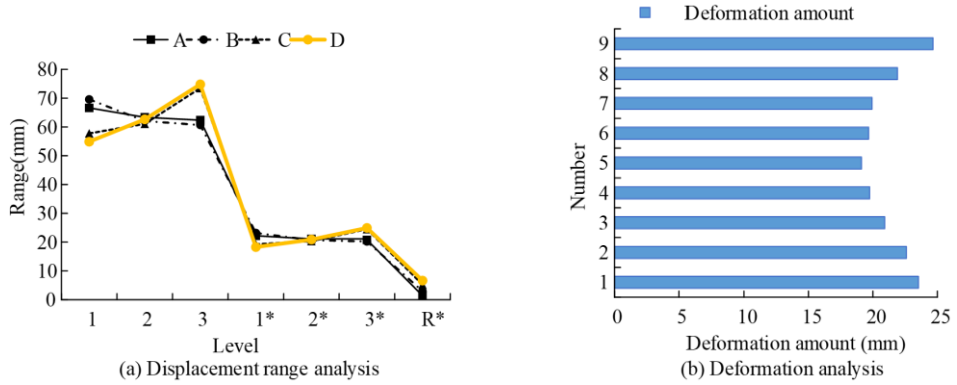

Fig. 6 Range of displacement and deformation of roadway rock layers

This study analyzed the four factors of length, diameter, spacing, and row spacing as the main influencing factors of the support structure, and designed parameter optimization schemes for nine support anchor rods based on the level of influencing factors. This study used orthogonal experiments to verify the influence of different factors on the optimization results of support structures, and at the same time, the range analysis method was used to process the results. Statistics and analysis of different factors at different levels of experimental results could evaluate the degree to which these factors affect the experimental results. The specific results are shown in Table 4.

From Table 4, there were significant differences in the total displacement of each factor at different levels. Factor D (spacing) had the highest total displacement at level 3 (74.79 mm) and the lowest displacement at level 1 (54.88 mm). The average displacement increased from 18.29 mm at level 1 to 24.93 mm at level 3, with an average range of 6.64 mm, which is the largest among the four factors. This indicated that spacing had the most significant impact on the deformation of NMR rock formations. In terms of the horizontal priority, the displacement of factors A and B showed a decreasing trend with increasing horizontal level (level 1>level 2>level 3), indicating that the larger the length and diameter of the anchor rod, the smaller the rock displacement. The displacement of factors C and D showed an upward trend with increasing horizontal direction (level 3>level 2>level 1), indicating that the larger the spacing and row spacing, the greater the rock displacement. In summary, the primary and secondary order of the influence of various factors on the displacement of NMR rock layers is spacing (D)>spacing(C)>diameter (B)>length (A). Afterwards, the study verified the specific results of the range of rock displacement in the roadway, as shown in Fig.6.

In Table 6, A, B, C, and D are the four influencing factors of the length, diameter, spacing, and row spacing of the support anchor rods. The horizontal axis 1-3 represents the sum of displacement at different parameter levels, 1*-3* represents the average displacement at different parameter levels, and R* represents the average. In Fig.6 (a), the average displacement range of A, B, C, and D in NMTs was 1.42 mm, 2.97 mm, 5.24 mm, and 6.64 mm, indicating that the spacing factor has the greatest impact on rock deformation, followed by the spacing factor. In Fig.6 (b), among the 9 optimization parameters, Scheme 5 had the smallest deformation of the rock layer under the support structure. Therefore, in the NMR of the mine, it was necessary to adjust the anchor rod's length in the support structure to 140 cm, the anchor rod's diameter to 18 mm, the spacing to 110 cm, and the row spacing to 100 cm. Afterwards, this study analyzed the optimization of the support of the mining roadway, and the LZR of the rock strata in the mining roadway was 1.0m-1.5m. Table 5 shows the factors, levels, and optimization parameters of the mining roadway support structure.

Table 5. Optimization test parameters of mining tunnel support structure

	Factors and levels				Optimization plan								
Factor	Code	Level1	Level2	Level3	1	2	3	4	5	6	7	8	9
Length (cm)	A	160	180	200	160	160	160	180	180	180	200	200	200
Diameter (mm)	B	16	18	20	16	18	20	16	18	20	16	18	20
Distance (cm)	C	90	100	110	90	110	100	110	100	90	100	90	110
Row spacing (cm)	D	90	100	110	90	100	110	110	90	100	100	110	90

Based on the data in Table 5, orthogonal experiments and range analysis methods were used to obtain the results, as shown in Fig.7.

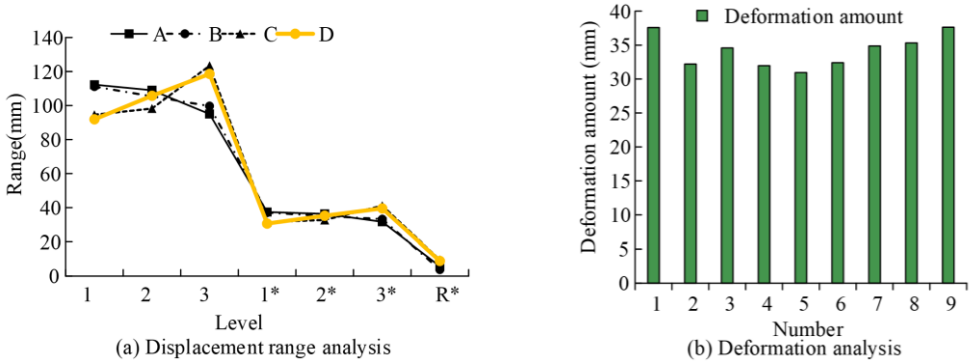

(a) Displacement range analysis (b) Deformation analysis

Fig. 7 Range of rock displacement and deformation in mining tunnels

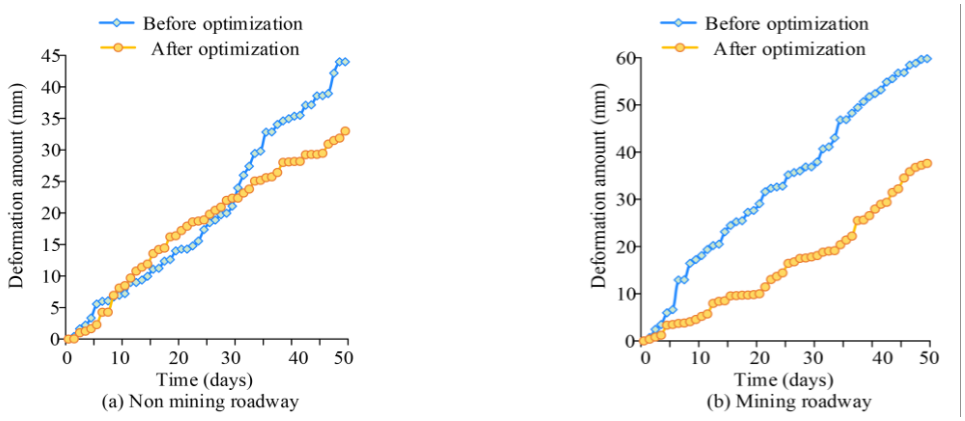

(a) Non mining roadway (b) Mining roadway

Fig. 8 The subsidence and deformation of the top rock strata in mining tunnels under different support structure environments

Table 6. ANOVA results of support structure parameters in mining roadway

Source of Variation	Sum of Squares	Degrees of Freedom	Mean Square	F	*p*
Length (A)	32.45	2	16.23	8.92	0.009
Diameter (B)	15.28	2	7.64	4.20	0.048
Spacing (C)	92.16	2	46.08	25.34	<0.001
Row spacing (D)	78.54	2	39.27	21.59	<0.001
Error	14.55	8	1.82	/	/
Total	232.98	16	/	/	/

In Fig.7 (a), the average displacement range of A, B, C, and D in NMTs was 5.74 mm, 3.82 mm, 9.6 mm, and 8.9 mm, indicating that the spacing factor has the greatest impact on rock deformation, followed by the spacing factor. In Fig.7 (b), among the 9 optimization parameters, Scheme 5 had the smallest deformation of the rock layer under the support structure. Therefore, in the mining roadway of the mine, the length of the anchor rod in the support structure was adjusted to 180 cm, the diameter was adjusted to 18 mm, the spacing was adjusted to 100 cm, and the row spacing was adjusted to 90 cm. Finally, this study detected the deformation of the top rock strata of the mine roadway under different support structure environments, as shown in Fig.8.

In Fig.8 (a), before optimizing the support structure, the maximum settlement of the top rock layer of the NMR in the mine was 43.93 mm. After optimizing the support structure, the maximum settlement was 32.74 mm. In Fig.8 (b), before optimizing the support structure, the maximum settlement of the top rock layer of the mining roadway in the mine was 59.81 mm, and after optimizing the support structure, the maximum settlement was 37.66 mm. To further evaluate the statistical significance of the influence of different support structure parameters on rock deformation, the study used Analysis of Variance (ANOVA) to test the results of orthogonal experiments, as shown in Table 6.

From Table 6, in mining tunnels, the p-values of spacing, row spacing, and length were all less than 0.01, indicating a highly significant impact. The p of the diameter was less than 0.05, indicating a significant impact. Among them, the F-value of the spacing was the highest (25.34), indicating that it has the most significant impact on rock deformation, which is highly consistent with the range analysis results in Fig.7 (a) (the average range of spacing is 9.6 mm). In summary, the results of the ANOVA validated the reliability of the range analysis in orthogonal experiments and clarified the statistical significance of the influence of various support structure parameters on rock deformation. This analysis provided a statistical basis for the parameter optimization of mine roadway support structure, enhancing the credibility and scientific of the optimization results.

Overall, in NMTs, the spacing of support structures has the most significant impact on rock displacement, and displacement increases with the increase of spacing. This result is highly consistent with the mechanical mechanism of anchor rod support: the increase in the spacing and row spacing of anchor rods means that the number of anchor rods per unit area is reduced, the support density is reduced, and the reinforcement effect of anchor rods on the surrounding rock is weakened. This results in a decrease in the self-supporting ability of the surrounding rock and causes greater deformation of the rock formation. For NMTs, the parameters of the optimized plan are: anchor rod length of 140 cm, diameter of 18 mm, spacing of 110 cm, and row spacing of 100 cm. Compared with the original design plan (anchor rod length of 120 cm, diameter of 16 mm, spacing of 100 cm, row spacing of 100 cm), the optimized plan increases the anchor rod length by 20 cm, diameter by 2 mm, but spacing by 10 cm. The number of anchor rods per unit area decreases from 1.0 per square meter (spacing of 100 cm × row spacing of 100 cm) in the original plan to 0.91 per square meter (spacing of 110 cm × row spacing of 100 cm), a decrease of about 9%. Taking into account material costs and construction quantities, the optimized plan significantly reduces rock displacement (by 25.5%) while also lowering support density, demonstrating good economic viability.

4. Conclusion

The study used the stochastic gradient descent algorithm to optimize the BP neural network model (SGD-BP) for predicting the range of loose zones in the surrounding rock of mining tunnels, and based on the prediction results, guided the optimization of support structure parameters. Through theoretical analysis and experimental verification, the following main conclusions are drawn:

1. In terms of model parameter optimization, when the learning rate of the SGD-BP model is set to 0.001, the prediction error is between 1.0 cm and 2.9 cm, with an average error of 2.06 cm. When the number of hidden layer neurons is set to 25, the average error is further reduced to 1.43 cm. Under the above parameter combination, the model has the best prediction performance.
2. In terms of model prediction accuracy, the absolute prediction error of the SGD-BP model is in the range of 1.92 cm to 6.10 cm, with an average prediction error of 3.91 cm and the highest error proportion of 4.9%. In contrast, the absolute prediction error of PSO-BP is in the range of 3.01 cm to 12.70 cm, with an average prediction error of 7.22 cm and a maximum error proportion of 11.1%. The experimental results show that the SGD-BP model has higher accuracy and lower errors in predicting the LZR of mines.
3. In terms of the optimization effect of the support structure, before optimization, the maximum settlement of the rock layer at the top of the NMR is 43.93 mm, while at the top of the mining roadway is 59.81 mm. After optimization, the maximum settlement of the rock layer at the top of the NMR decreases to 32.74 mm (a decrease of 25.5%), and that at the top of the mining roadway decreases to 37.66 mm (a decrease of 37.0%). The experimental results show that the optimization of support parameters guided by the prediction results of the SGD-BP model can significantly reduce the settlement deformation of the rock strata at the top of the roadway.
4. In terms of sensitivity of support parameters, the range analysis results show that the spacing factor has the greatest impact on the settlement displacement of the top support structure in mining tunnels, with an average displacement range of 9.6 mm. The spacing factor has the greatest impact in NMTs, with an average displacement range of 6.64 mm. The optimized support parameters are anchor rod length of 180 cm, diameter of 18 mm, spacing of 100 cm, and spacing of 90 cm in mining tunnels; anchor rod length of 140 cm, diameter of 18 mm, spacing of 110 cm, and spacing of 100 cm in NMTs.

The limitation of the study lies in the simplification of the support structure in the analysis of mechanical characteristics, without fully considering the anisotropy and nonlinear characteristics of rock layers under complex geological conditions. Future research will be based on the actual geological conditions of the mine, establish more refined numerical models, and combine them with more on-site monitoring data for model validation and optimization.

References

Alesmael, A., & Ekmen, A. B. (2025). Artificial intelligence supported optimization of piled raft foundations based on three-dimensional finite element analyses. Structures, 77, 109210. https://doi.org/10.1016/j.istruc.2025.109210

Avci, Y., & Ekmen, A. B. (2023). Artificial intelligence assisted optimization of rammed aggregate pier supported raft foundation systems based on parametric three-dimensional finite element analysis. Structures, 56, 105031. https://doi.org/10.1016/j.istruc.2023.105031

Ding, G., Duan, Y. Q., Han, G., Zhao, Q., Ma, P., & Zhang, D. (2024). Study on roadway layout and supporting method of high intensity mining disturbance bottom coal recovery working face (A case study in Xiagou mine). International Journal of Oil, Gas and Coal Engineering, 2(3), 63-74. https://doi.org/10.11648/j.ogce.20241203.11

Dong, H., Zhang, J., & Zhang, F. (2022). Study on deformation and supporting measures of mining roadway with compound roof. 40(3), 1449-1462. https://doi.org/10.1007/s10706-021-01974-x

Han, H., Ma, W., Bao, W., Wu, H., Li, R., & Xu, T. (2025). Cross-validated GA-BP model for anomaly detection in deformation monitoring using GNSS and accelerometer data. IEEE Sensors Journal, 25(13), 24748-24762. https://doi.org/10.1109/JSEN.2025.3567176

Islavath, S. R., & Deb, D. (2022). Interaction of a shield structure with surrounding rock strata under geo-static and fatigue loadings. Geotechnical and Geological Engineering, 40(6), 2949-2965. https://doi.org/10.1007/s10706-022-02072-2

Jha, M. K. (2025). Machine learning applications for roadway pavement deterioration modeling. Journal of Computational and Cognitive Engineering, 4(1), 47-55. https://doi.org/10.47852/bonviewJCCE32021985

Li, C., Jia, T., Han, X., & Jiang, X. (2023). Study on parameter optimization of laser cladding Fe60 based on GA-BP neural network. Journal of Adhesion Science and Technology, 37(18), 2556-2586. https://doi.org/10.1080/01694243.2022.2159298

Li, C., Li, Z., & Li, Y. (2024). Railway wireless train communication network scheduling based on GA-BP algorithm. International Journal of Reasoning-Based Intelligent Systems, 16(4), 278-288. https://doi.org/10.1504/IJRIS.2024.142356

Li, S., Li, C., Wang, X., Liu, P., & Han, X. (2025). Evaluation and analysis of particle oxidation of HVOF thermal spraying based on GA-BP neural network algorithm. Journal of Thermal Spray Technology, 34(1), 267-290. https://doi.org/10.1007/s11666-024-01906-0

Liu, S., & Zhang, J. (2022). Research on dynamic stability of large deformation roadway with application of segmented resistance anchor bolt. Journal of Vibroengineering, 24(8), 1461-1470. https://doi.org/10.21595/jve.2022.22677

Liu, Y., Liu, J., Zhang, F., & Li, W. (2022). Evolution of excavation-induced critical stress ring and corresponding support of deep roadway. Arabian Journal of Geosciences, 15(1), 118-1-118-14. https://doi.org/10.1007/s12517-021-09301-7

Rabbani, A., Muslih, J. A., Saxena, M., Patil, S. K., Mulay, B. N., Tiwari, M., & Samui, P. (2024). Utilization of tree-based ensemble models for predicting the shear strength of soil. Transportation Infrastructure Geotechnology, 11(4), 2382-2405. https://doi.org/10.1007/s40515-024-00379-6

Rabbani, A., Samui, P., & Kumari, S. (2023). Optimized ANN-based approach for estimation of shear strength of soil. Asian Journal of Civil Engineering, 24(8), 3627-3640. https://doi.org/10.1007/s42107-023-00739-6

Rabbani, A., Samui, P., Kumari, S., Saraswat, B. K., Tiwari, M., & Rai, A. (2024). Optimization of an artificial neural network using three novel meta-heuristic algorithms for predicting the shear strength of soil. Transportation Infrastructure Geotechnology, 11(4), 1708-1729. https://doi.org/10.1007/s40515-023-00343-w

Wang, Z., Long, M., Duan, W., Wang, A., & Li, X. (2024). Predicting the residual strength of oil and gas pipelines using the GA-BP neural network. Recent Innovations in Chemical Engineering, 17(3), 233-254. https://doi.org/10.2174/0124055204315589240502052118

Wu, H., Sun, C., Lu, Q., Wang, Y., Liu, Y., Zou, L., & Tan, J. (2025). Unbalance prediction method of aero-engine saddle rotor based on deep belief networks and GA-BP intelligent learning. Journal of Intelligent Manufacturing, 36(4), 2829-2840. https://doi.org/10.1007/s10845-024-02392-5

Xu, W., Wang, Z., Zhu, X., Zhang, B., Zheng, Z., & Lv, M., Wang, H. (2024). Intelligent optimization of cold radial forging process for 20CrMnTiH alloy based on GA-BP and performance analysis. The International Journal of Advanced Manufacturing Technology, 135(9/10), 4281-4307. https://doi.org/10.1007/s00170-024-14713-2

Yao, W., Liu, G., Pang, J., & Huang, X. (2023). Instability mechanism and surrounding rock control technology of roadway subjected to mining dynamic loading with short distance: A case study of the Gubei coal mine in China. Geotechnical and Geological Engineering, 41(2), 1407-1427. https://doi.org/10.1007/s10706-022-02343-y

Yuan, Y., Han, C., Zhang, N., Feng, X., Wang, P., Song, K., & Wei, M. (2022). Zonal disintegration characteristics of roadway roof under strong mining conditions and mechanism of thick anchored and trans-boundary supporting. Rock Mechanics and Rock Engineering, 55(1), 297-315. https://doi.org/10.1007/s00603-021-02653-2

Zhang, Z., Liu, H., Chen, H., Tan, S., & Tong, X. (2023). Study on supporting technology of a mining roadway in fault fracture zone with high altitude. Geotechnical and Geological Engineering, 41(3), 1839-1854. https://doi.org/10.1007/s10706-022-02375-4

Zhou, P., Zhou, F., Lin, J, Li, J. Y., Jiang, Y. F., Yang, B., & Wang, Z. J. (2021). Decoupling analysis of interaction between tunnel surrounding rock and support in Xigeda formation strata. KSCE Journal of Civil Engineering, 25(12), 4897-4912. https://doi.org/10.1007/s12205-021-0618-4

Zhou, Z., Chen, Z., He, C., Jiang, C., & Li, T. (2024). A solution method for a tunnel supporting structure system incorporating the active control of surrounding rock deformation. International Journal of Geomechanics, 24(1), 4023243.1-4023243.19. https://doi.org/10.1061/IJGNAI.GMENG-8652

Disclaimer